

Controlling Metamaterial Resonances with Light

Sangeeta Chakrabarti, S. Anantha Ramakrishna and Harshawardhan Wanare
Department of Physics, Indian Institute of Technology Kanpur 208016, India

We investigate the use of coherent optical fields as a means of dynamically controlling the resonant behaviour of a variety of composite metamaterials, wherein the metamaterial structures are embedded in a dispersive dielectric medium. Control and switching is implemented by coherently driving the resonant permittivity of the embedding medium by applied optical radiation. The effect of embedding Split ring resonators (SRR) in a frequency- dispersive medium with Lorentz-like dispersion or with dispersion engineered by electromagnetic induced transparency (EIT), is manifested in the splitting of the negative permeability band, the modified (frequency-dependent) filling fractions and dissipation factors. The modified material parameters are strongly linked to the resonant frequencies of the medium, while for an embedding medium exhibiting EIT, also to the strength and detuning of the control field. The robustness of control against the deleterious influence of dissipation associated with the metallic structures as well as the inhomogeneous broadening due to structural imperfections is demonstrated. Studies on plasmonic metamaterials that consist of metallic nanorods arranged in loops and exhibit a collective magnetic response at optical frequencies are presented. Control and switching in this class of plasmonic nanorod metamaterials is shown to be possible, for example, by embedding these arrays in a Raman active liquid like CS₂ and utilizing the Inverse Raman Effect.

PACS numbers: 81.05.Xj, 78.67.Pt, 41.20.Jb, 42.50.Ar

In recent times, several new developments have considerably altered our perception of the interaction of electromagnetic waves with material media in general and light-matter interaction in particular. On one hand, the coherent control of quantum systems utilizing the quantum interference route [1] has enabled researchers to demonstrate superluminal [2] and subluminal [3] propagation of light, stopped light [4, 5], render an opaque medium transparent at a designated frequency (Electromagnetically Induced Transparency or EIT) [6, 7] and generate an ultra-high index of refraction [8], while on the other, the development of structured composite media known as metamaterials [9] has opened up new possibilities like negative refraction [10, 11], perfect lenses [12], "invisibility cloaks" [13], etc. These effects have been realised using on two different approaches to the study of light-matter interaction. While coherent control is a purely quantum mechanical phenomenon, metamaterials can be analysed within the framework of classical electromagnetic theory.

One of the most attractive features of metamaterials, (whose resonant response is governed by their underlying geometric structure) is the fact that they can be designed to operate at any predetermined frequency. In addition, it is also possible to modify and control their response. However, the very resonant nature of the response of metamaterials that gives rise to their novel properties also hinders their applicability owing to the high levels of dissipation associated with their response. Although designing metamaterials that function at optical frequencies is difficult, it has been demonstrated by several groups [14]. Another drawback of metamaterials arises from the fact that since their response depends on their geometrical structure, their properties are fixed once they have been fabricated. However, to incor-

porate greater flexibility to their structure and performance, metamaterials need to be both reconfigurable as well as controllable. Recently, control of metamaterial response has been demonstrated, both by passive as well as dynamical methods [15–18].

In this paper, we demonstrate the possibility of controlling the magnetic response of metamaterials consisting of Split Ring Resonators (SRR) [19] by actively tuning the capacitance of these structures at near-infrared and optical frequencies. We have used the term metamaterial to signify the bare metamaterial while the term 'composite metamaterials' indicates metamaterials embedded in a dispersive background. Our approach to this scheme is both simple and straightforward. It makes use of quantum mechanical phenomena to parametrically control a purely classical effect. This is achieved by embedding the metamaterial within a coherent atomic/molecular medium. An appropriate choice of the resonance frequencies of the metamaterial and the embedding medium, together with the control field and its detuning (in the case of EIT) results in complete control of the effective magnetic response of the metamaterial. This occurs through the interaction of the narrow atomic resonance of the background dielectric with the broader magnetic resonance of the metamaterial. Along with the control over the magnetic response, it is seen that the dissipation inherent in the metamaterial can be reduced significantly. This scheme may be used to produce metamaterials which are reconfigurable as well as controllable by choosing a slightly different resonance frequency for the embedding medium. In addition, we also show how an array of nanorods that exhibits a magnetic response which is plasmonic in origin [20] can also be controlled via the self-capacitance of the array. Further, the same array of nanorods (which is known to behave

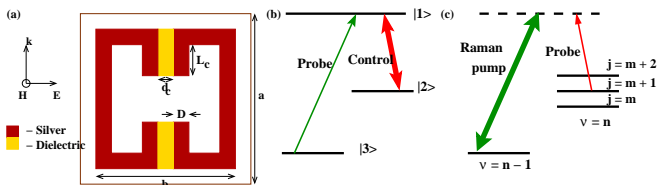


FIG. 1: Atomic level schemes for realizing (a) Lorentz permittivity dispersion (by means of a Raman transition) and (b) EIT-like permittivity dispersion. (c) The homogenizable SRR [21] used in our calculations. A slab consisting of these SRRs exhibits negative magnetic permeability in a frequency range above the magnetic resonance frequency $\omega_m = 1/\sqrt{LC}$. The following structural parameters are used in our calculations: $a = 600\text{nm}$, $b = 312\text{nm}$, $L = 144\text{nm}$, $d = 24\text{nm}$, $D = 24\text{nm}$.

like an effective plasma when radiation whose electric field is axially oriented is incident upon it), can be made transmittive at frequencies well below its effective plasma frequency via the resonantly enhanced permittivity of its background medium.

I. ANALYTICAL DESCRIPTION

Let us consider a metamaterial consisting of an array of symmetric split ring resonators (SRR), as shown in Fig. 1(a). These arrays lie in the horizontal plane and are stacked up vertically. The size of the individual inclusions ($\sim \lambda/10$) makes it possible to describe the array as an effective medium at the frequencies of interest. This medium has been shown to possess a resonant magnetic response and its effective permeability is μ_{bare} given by [21]:

$$\mu_{\text{bare}}(\omega) = 1 + \frac{f_m \omega^2}{\omega_m^2 - \omega^2 - i\Gamma_m \omega}. \quad (1)$$

Here, $\omega_m = \frac{1}{\sqrt{LC}}$ where L and C are the total inductance and the total capacitance of the structure [21], f_m is the filling fraction while the factor Γ_m , which governs the effective dissipation present in the SRR medium, is related to the intrinsic dissipation rate of the metal defined according to the Drude model for the dielectric permittivity. This medium exhibits a negative permeability leading to a band gap in a frequency range above ω_m if Γ_m is small enough. We study the effect of embedding an array of such SRRs in a medium having a frequency-dispersive dielectric permittivity. This may either be a resonant Lorentz-type dispersion, or under the application of a pair of coherent control and probe fields, EIT-like. In the first case, the relative permittivity of the medium is given by the expression

$$\epsilon(\omega) = 1 + \frac{f_e^2}{\omega_e^2 - \omega^2 - i\gamma_e \omega}, \quad (2)$$

where $f_e^2 = Ne^2/m\epsilon_0$ (N is the density of (atomic) oscillators, ϵ_0 is the permittivity of free space while e and m are the electronic charge and mass, respectively), ω_e is the dielectric resonance frequency and γ_e is the dissipation factor. Such a dispersion can be realized by using for example, resonant quantum dots or choosing a Raman transition [22] with a strong pump field ensuring that the resonant Raman probe frequency is close to the magnetic resonance frequency of the metamaterial, ω_m .

In the second case, when the medium exhibits EIT, the permittivity for the probe field is given by [23]

$$\epsilon_{\text{EIT}}(\omega) = 1 + \frac{\kappa(\omega_1 - \omega)}{(\omega_1 - \omega)^2 - \frac{\Omega_c^2}{4} - i\gamma_{13}(\omega_1 - \omega)}. \quad (3)$$

Here $\omega_1 = \frac{E_1 - E_3}{\hbar}$, Ω_c is the Rabi frequency of the control field defined as $\Omega_c = \frac{\vec{d}_{12} \cdot \vec{E}}{\hbar}$, $\kappa = (N_a |d_{13}|^2)/(\epsilon_0 \hbar)$ is the strength of the transition, N_a is the atomic density, γ_{13} and d_{13} represent the decay rate and the dipole moment, respectively, between the atomic levels $|1\rangle$ and $|3\rangle$ while d_{12} represents the dipole moment between levels $|1\rangle$ and $|2\rangle$ (see Fig. 1(b)). It should be noted that in the absence of the control field, the dispersion obtained is the same as in the case of the Lorentz permittivity.

In the presence of the embedding medium, the capacitance of individual SRR units becomes strongly frequency-dependent. This makes the resonance frequency of the composite medium (ω_{eff}) appear frequency dispersive as: $\omega_{\text{eff}} = \frac{\omega_m}{\sqrt{\epsilon(\omega)}}$.

The sharply resonant nature of $\epsilon(\omega)$ results in the SRR medium showing a resonant magnetic response at multiple frequencies. These predominantly occur above and below ω_m , depending on whether the frequency of the incident wave is greater than or lesser than ω_e . The new resonance frequencies are the solutions of the transcendental equation

$$\text{Re}[\omega_m^2/\epsilon(\omega)] - \omega^2 = 0, \quad (4)$$

while $\text{Im}[\omega_m^2/\epsilon(\omega)]$ quantifies the dissipation in the effective medium. Essentially, the presence of the dispersive dielectric permittivity of the embedding medium turns the SRR into a resonantly driven, actively tuned LC-circuit. The capacitance of the LC-circuit becomes frequency dependent, allowing the satisfaction of the resonance conditions Eq. (4) at multiple frequencies with the corresponding negative- μ band gap of the ‘bare’ SRR splitting into two or more band gaps.

The filling fraction f_{eff} and the dissipation parameter of the composite metamaterial can be viewed as effective frequency dependent quantities whose behaviours are greatly influenced by the resonant background. The effective filling fraction f_{eff} and the effective dissipation parameter Γ_{eff} have the following generic forms in the presence of a frequency-dispersive background:

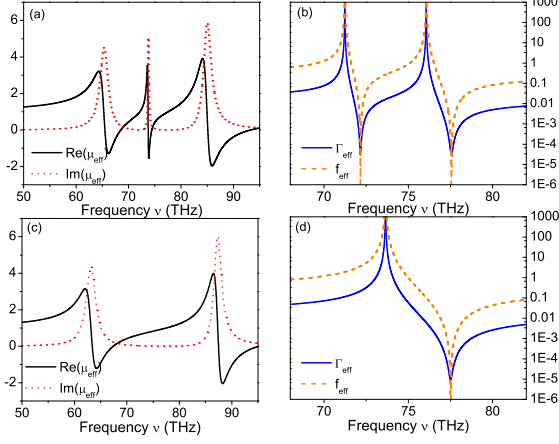


FIG. 2: (a) The frequency dependent μ_{eff} and (b) Γ_{eff} and filling fraction f_{eff} (obtained analytically) for the SRR metamaterial in the presence of an embedding dielectric medium displaying EIT. (c) and (d): The same quantities for the SRR metamaterial embedded in a medium which has a resonant Lorentz permittivity.

$$f_{\text{eff}}(\omega) = f_m [\{\text{Real}[\epsilon(\omega)]\}^2 + \{\text{Im}[\epsilon(\omega)]\}^2], \quad (5)$$

$$\Gamma_{\text{eff}}(\omega) = \omega_m^2 \frac{\text{Im}[\epsilon(\omega)]}{\omega} + \Gamma_m \{\text{Real}[\epsilon(\omega)]\}^2 + \Gamma_m \{\text{Im}[\epsilon(\omega)]\}^2. \quad (6)$$

Let us now study the effect of the Lorentz and the EIT dispersion on the properties of the metamaterial in some detail. If the background dielectric medium has a Lorentz-type dispersion, the following expressions for f_{eff} and Γ_{eff} are obtained:

$$f_{\text{eff}} = f_m \left[1 + \frac{f_e^2(2(\omega_e^2 - \omega^2) + f_e^2)}{(\omega_e^2 - \omega^2)^2 + (\gamma_e \omega)^2} \right], \quad (7)$$

$$\Gamma_{\text{eff}} = \Gamma_m + \frac{\Gamma_m f_e^2(2(\omega_e^2 - \omega^2) + f_e^2) + \omega_m^2 f_e^2 \gamma_e}{(\omega_e^2 - \omega^2)^2 + (\gamma_e \omega)^2}. \quad (8)$$

Along with the two new magnetic resonance frequencies and a split in the negative μ -band, a region of significantly reduced absorption is observed between the two resonances. In fact, the $\text{Im}[\mu_{\text{eff}}]$ is observed to pass through a minimum at the resonant frequency of the bare SRR if $\omega_m = \omega_e$. There is also a significant change in the nature of f_{eff} and Γ_{eff} around the frequency ω_e . The large values of f_{eff} at ω_e is due to the resonant enhancement of the cross-section of the SRR structural unit: the SRR appear much larger to radiation at resonance than they actually are. The reduction in absorption at ω_e is due to the vanishing of the currents in the SRR. This results from an interplay of two currents giving rise to different charge densities. The first of these is due to the

current induced in the SRR unit by the magnetic field of the incident radiation. The second arises due to electric polarization of the embedding dielectric background by the electric field of the incident light. At resonance, the two are out of phase with each other leading to the freezing of currents in the SRR. The proximity of ω_e to ω_m determines the extent of modulation of the μ_{eff} response. In other words, the interaction between the electric and magnetic resonances is the strongest when ω_e lies in the vicinity of ω_m , ($\omega_m \pm \Gamma_m$). Otherwise, the two resonances are virtually uncoupled.

The magnetic response of the composite metamaterial embedded in an EIT medium exhibits multiple magnetic resonances (Fig. 2(b)). This is again accompanied by drastically reduced absorption within two frequency bands. The strength and the detuning of the control field can both be used to shift the positions, widths, slopes and dissipation associated with the various resonances in μ_{eff} . In fact, this scheme is more amenable to control as compared to the one described earlier because the detunings of the probe and the control beams (both positive and negative) can be used to shift the EIT line centre and hence, the frequencies at which the absorption in the metamaterial is reduced. Again, the effective filling fraction and the modified dissipation parameter are given by

$$f_{\text{eff}} = f_m \left[1 + \frac{\kappa \Delta (2(\Delta^2 - \Omega_c^2) + \kappa \Delta)}{(\Delta^2 - \Omega_c^2/4)^2 + (\gamma_{12} \Delta)^2} \right], \quad (9)$$

$$\Gamma_{\text{eff}} = \Gamma_m + \frac{\Gamma_m \kappa \Delta (2(\Delta^2 - \Omega_c^2) + \kappa \Delta) + \omega_m^2 \kappa \Delta \gamma_{12}}{(\Delta^2 - \Omega_c^2)^2 + (\gamma_{12} \Delta)^2}, \quad (10)$$

where $\Delta = \omega_1 - \omega$.

From the preceding expressions, we find that the new filling fraction f_{eff} increases close to the resonant frequency while Γ_{eff} exhibits sub-natural ($\Gamma_{\text{eff}} \ll \Gamma_m$) values around the atomic resonances (Fig. 2(c)). At the EIT line centre frequency (ω_1), f_{eff} and Γ_{eff} are found to have the same values as the bare SRR medium. As before, the reduction in absorption is a manifestation of the vanishing currents in the SRR loops. It is interesting to note that if losses are reduced significantly, the regions where $\text{Re}[\mu_{\text{eff}}] < 0$ gradually disappear, (see Fig. 2), in agreement with the findings of Stockman [24].

If the metamaterial has been designed to exhibit a resonant response at the frequency of the EIT line centre in the absence of medium, the resonant magnetic response of the composite metamaterial is found to be such that $\text{Re}[\mu_{\text{eff}}] \rightarrow 1$ (with an associated imaginary part) exactly at the EIT line centre. However, if $\omega_m \neq \omega_1$, the response of the composite at the EIT line centre is simply the value of μ_{bare} at the frequency ω_1 . It should be emphasized that since we are dealing with a resonant system with a highly dispersive lineshape, changes of the control parameter (ϵ_L or ϵ_{EIT}) can lead to large-scale changes in response (μ_{eff}) at a given frequency, due to the shift in the resonance frequency.

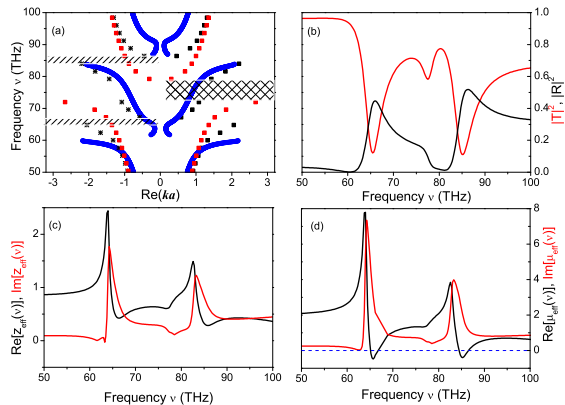


FIG. 3: (a): The computed band structures for the bare SRR (red circles) and the composite metamaterial embedded in a Raman medium (black squares) under the condition $\omega_e = \omega_m$. The blue lines represent the dispersion predicted by the analytic formula. The band gaps due to $\mu_{\text{eff}} < 0$ are indicated by the cross-hatched region on the right (for the bare SRR whose $\omega_m = 74.9\text{THz}$) and the two hatched regions on the left (for the band gaps resulting from the inclusion of the resonant Raman medium).

(b) The reflectivity and the transmittivity for a calculated for a slab consisting of a single layer of SRR. Note the presence of two stop bands (low $|T|^2$) corresponding to the band gap frequencies in (a) and the new transmittive band that develops within the original band gap.

(c) The effective impedance $Z(\nu)$ of the composite metamaterial showing the presence of two resonances.

(d): The μ_{eff} , for a slab of the SRR metamaterial with an embedded resonant medium, retrieved using the computed reflection and the transmission coefficients. Note the existence of two frequency ranges where $\mu_{\text{eff}} < 0$. The grey dotted line represents the zero level.

II. NUMERICAL SIMULATION OF THE SRR METAMATERIAL AT MID-IR FREQUENCIES

Numerical simulations using the PHOTON codes based on the Transfer Matrix Method [25, 26] were carried out to verify our theoretical predictions. We present the canonical example of subwavelength-sized SRR made of silver at mid-infrared (mid-IR) frequencies. The metamaterial shows magnetic activity for applied radiation polarized with the magnetic field along the SRR axis. The structures were modelled as being embedded in a resonant background. We have used experimentally obtained parameters for silver [27] in our calculations. (We use silver for all metallic inclusions in this paper.)

The cross-section of the (cylindrical) SRR that we considered in this case is shown in Fig. 1. Seventy-five grid points along each direction were used for computing the band structure as well as the reflection and the transmission coefficients. Invariance along the cylindrical axis is assumed. The bare SRR in this case has a magnetic resonance frequency of 74.9 THz. This metamaterial contain-

ing a Lorentz-type dielectric within its capacitive gaps is modelled using the following parameters: $f_e = 24.1\text{ THz}$, $\omega_e = 74.9\text{ THz}$ and $\gamma_e = 2.4\text{ THz}$.

As predicted in the preceding section, the negative μ band splits in the presence of the embedding dielectric medium. The frequencies at which the new band gaps are formed are consistent with the predicted values. The mismatch between the results of the TMM calculation and the analytic formula can be attributed to the presence of parasitic capacitances in the SRR. These capacitances, which were neglected in the theoretical model used to describe the functioning of the SRR [21], are automatically taken into account in the TMM simulation.

The results of the band structure calculation were compared with the transmittivity and the reflectivity calculated for a slab consisting of a single layer of the SRR. A new propagating band (indicated by a peak in the transmittivity) is found to occur within the stop band region of the bare SRR. The frequency intervals corresponding to the new band gaps (regions of high reflectivity and low transmittivity) were found to be consistent with the band structure calculations. To illustrate the splitting of the negative permeability band, the effective material parameters for a slab consisting of four layers of the SRR-dielectric composite were determined using a retrieval procedure that utilizes the complex reflection and transmission coefficients [28]. The splitting of the negative μ band is found to be consistent with the predicted values (Fig. 3 (d)) and also with the simulated band structure and the reflectivity and the transmittivity. In addition, Fig. 3(c) shows the effective impedance $Z(\nu)$ of the metamaterial, with two resonances at the same frequencies as the negative permeability bands, in contrast with the single peak in $Z(\nu)$ observed for the bare SRR[21].

Fig. 4 illustrates the response of the metamaterial when the dielectric and the magnetic resonances do not coincide, i.e., $\omega_e \neq \omega_m$. As before, the negative permeability band splits, but the new resonances are either red-shifted or blue-shifted (with respect to those obtained when $\omega_e = \omega_m$), depending on whether $\omega_e < \omega_m$ or $\omega_e > \omega_m$. A study of the reflection and transmission coefficients for a slab consisting of four layers of the SRR further confirms this behaviour. As seen in the case when $\omega_m = \omega_e$, two regions of enhanced reflectivity (corresponding to the band gaps) separated by a transmittive region (corresponding to the additional propagating band that develops) are observed. For multiple layers, additional peaks due to Fabry-Pérot resonances (arising as a result of multiple scattering) are observed. In each case, the calculated effective impedance ($Z(\nu)$) of the structure (not shown here) reveals the presence of two peaks, signifying the two magnetic resonances. However, the effect of the resonant Lorentz medium weakens considerably when the two resonances are far apart.

In a similar fashion, appropriately designed SRR structures, embedded in resonant atomic media, can be shown to behave in the same way at NIR/optical fre-

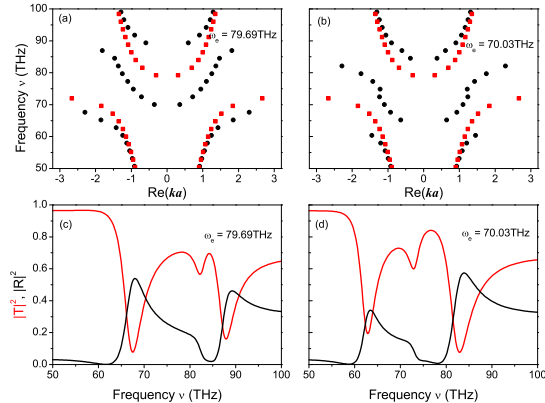


FIG. 4: The band structures and $(|T|^2, |R|^2)$ for the composite metamaterial when $\omega_m \neq \omega_e$.

(a): Band structure of the composite metamaterial when $\omega_e = 79.69\text{THz}$. The resulting gaps are blue-shifted with respect to those obtained when $\omega_e = \omega_m$.

(b): Band structure of the composite metamaterial when $\omega_e = 70.03\text{THz}$. In this case, the resulting gaps are red-shifted with respect to those obtained when $\omega_e = \omega_m$.

(c) & (d): Reflectivity and transmittivity calculated for a slab consisting minima in $|T|^2$ correspond to the new band gaps.

quencies [29]. Multiple layers of such SRR can switch sharply between highly reflecting to transmitting states within a narrow bandwidth. These fine features in the $|R|^2 - |T|^2$ profile arise due to the Fabry-Pérot resonances of the slab. Coupled with the control possible via EIT, these materials are potential candidates for narrow-band switching applications.

III. ROBUSTNESS OF THE CONTROL

Although it is often seen that light interacting with mesoscopic metallic structures experience much higher dissipation than the bulk metal itself, we have found that our results remain unaffected even if the intrinsic dissipation of the metal (silver, in this case) is increased three times from its bulk value.

There is another aspect of these structures that needs to be taken into account. The resonance frequency of these metamaterials depends crucially on the accuracy with which they can be fabricated. Thus, in practice, each metamaterial unit will be different from the rest, leading to a distribution of resonance frequencies rather than a single resonance frequency. The consequent broadening of the magnetic resonance could wipe out the narrow band effects predicted. Fortunately, we find that the effects are rather robust against the such inhomogeneous broadening.

We consider a distribution of magnetic resonance frequencies arising due to structural imperfections to be normally distributed (Gaussian) about the mean frequency

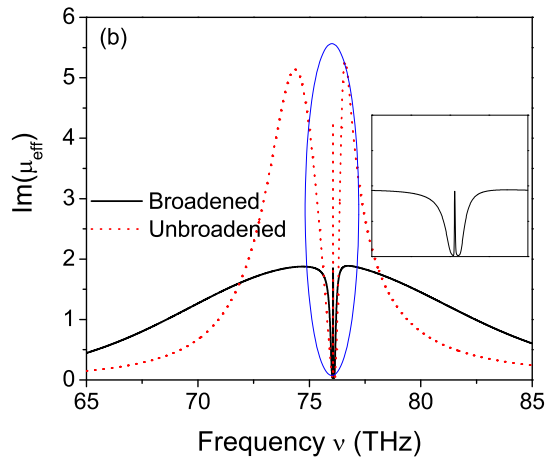
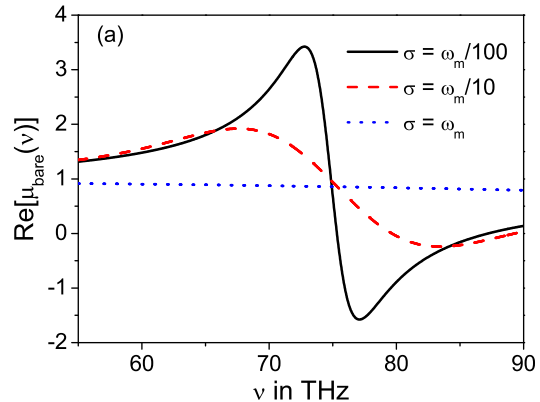


FIG. 5: (a) The effective permeability of the metamaterial for different widths of the distribution of the magnetic resonance frequency. The resonant μ_{eff} is washed out when the imperfections lead to $\sigma \sim \omega_m$.

(b): The broadened $\text{Im}(\mu_{\text{eff}})$ of the metamaterial in the presence of a background medium which exhibits EIT, for $\sigma = \omega_m/100$. The inset shows the details of the central part of the figure where the narrow features are seen to survive in spite of the broadening of the overall response.

ω_m . The width of this distribution (σ) is indicative of the extent of the imperfect structuring. Averaging over this distribution, we obtain:

$$\langle \omega_{\text{eff}}^2 \rangle = \omega_{\text{eff}}^2 + \frac{\epsilon_R \sigma^2}{\epsilon_R^2 + \epsilon_I^2} \quad (11)$$

$$\langle \Gamma_{\text{eff}} \rangle = \Gamma_{\text{eff}} + \frac{\epsilon_I \sigma^2}{\epsilon_R^2 + \epsilon_I^2} \quad (12)$$

$$\langle f_{\text{eff}} \rangle = f_{\text{eff}} \quad (13)$$

Note that the effective filling fraction (f_{eff}) remains unaltered. Thus, the effective permeability of the medium is found to broaden, as shown in Fig. 5(a).

For values of $\sigma \sim \Gamma_m$, we find that the narrow band effects arising due to the presence of $\epsilon(\omega)$ survive (See Fig.

5(b)). While the strength of the resonance decreases on the whole due to the larger Γ_{eff} , the regions of reduced absorption between the resonances remain nearly unaltered. The ‘increased’ filling fraction that remains unaffected by the inhomogeneous broadening compensates for the effect of the imperfections. In other words, the few resonant SRR units exhibit a large enough absorption cross-section such that the reduced number of participating SRRs due to the inhomogeneous broadening does not adversely affect the response on an average. Although accuracy in fabrication still remains an important issue, we note that the controllable effects discussed here are robust and generic to many metamaterials that depend upon resonances for their electromagnetic properties.

IV. PLASMONIC METAMATERIAL AT VISIBLE FREQUENCIES

In this section, we present the response and control of a metamaterial consisting of plasmonic nanorod loop inclusions. Arrays of small resonant plasmonic spheres arranged on subwavelength-sized loops have been shown to exhibit a magnetic response in Ref. [20]. We consider here plasmonic inclusions of metallic (silver) nanorods arranged on the circumference of a circle (Fig. 6(a)). The magnetic field of the incident radiation is assumed to be oriented along the axis of the rods. On assuming invariance along the rod axis, the problem becomes essentially two-dimensional. The loop exhibits a magnetic resonance that stems from an interaction driven by the individual plasmonic resonance of each nanorod. Each resonating nanoparticle induces a circulating *displacement* current around this loop. The electric dipole moments (perpendicular to the axis) tend to align along the circumference of the ring when driven at the plasmon resonance frequency. This is confirmed by our COMSOL finite elements numerical simulations (Fig. 6(b)) where an enormous confined magnetic field appears in the interior of the loop at resonance, when driven by an external source.

The size of the loop does not strongly influence the frequency of the individual magnetic resonance occurs. The plasmonic resonance frequency of each nanoparticle primarily determines the resonant behaviour of the loop. However, the number of plasmonic particles on the loop determines the strength of the resonance [20]. At resonance, the size of each unit cell ($a \sim \lambda/5$) and each loop inclusion is much smaller compared to the wavelength of the incident light ($R \sim \lambda/25$). Thus, Bragg scattering does not play a dominant role in the observed phenomenon and the system is easily homogenized.

The response of an array of such plasmonic loops was calculated using the PHOTON codes. The calculations are essentially two dimensional, the cylindrical axis being the axis of invariance. To avoid staircasing effects with a square grid, we considered rods with square cross-sections rather than circular ones. The unit cell is a square with

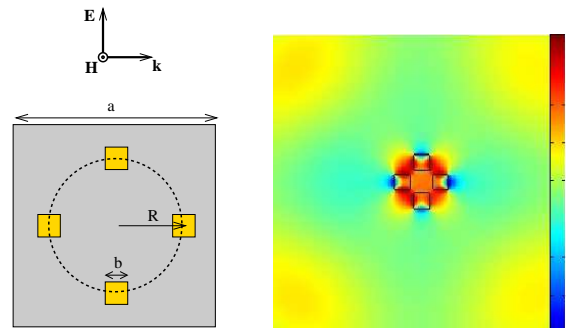


FIG. 6: (a): A cross-sectional view of a typical unit cell of the plasmonic loop metamaterial. The picture shows the nanorods placed on the circumference of a circle. The grey area represents the embedding dielectric medium. (b): The magnetic response of an isolated loop inclusion illustrating the concentration of the magnetic field inside the loop at resonance, when excited by means of a line source.

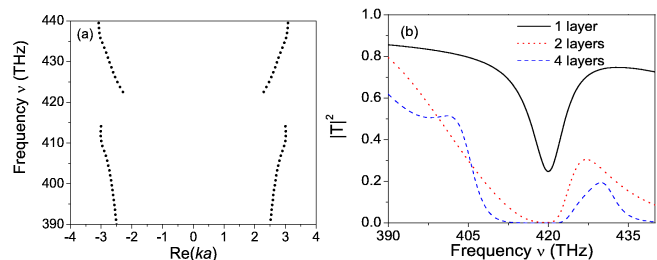


FIG. 7: (a) The band structure and (b), the transmittivity for four layers of unit cells of the plasmonic metamaterial. The additional peaks are the Fabry-Pérot resonances occurring due to multiple scattering between the interface of the medium and vacuum.

side $a = 150\text{nm}$ (See Fig. 6(a)). Within each unit cell of the metamaterial, four silver nanorods (of square cross-section and side $b = 25\text{nm}$), embedded in a background dielectric medium with $\epsilon_b = 2.65$, are symmetrically arranged on the circumference of a circle of radius $R = 26\text{nm}$. The metamaterial exhibits a distinctly identifiable magnetic resonance at $\sim 415\text{THz}$, with a negative magnetic permeability band gap up to $\sim 421\text{THz}$. This behaviour is also confirmed by the transmittivity for a slab composed of four layers of unit cells (loops) (Fig. 7(b)). We note that the resonance frequency of the metamaterial differs from that of the individual loop inclusions due to coupling between the nanoparticles. For smaller unit cell sizes and larger loop radii, the coupling between neighbouring plasmonic loop resonances leads to the hybridization of bands. Many weak resonances are found to occur close together and identification of the magnetic resonance leading to the negative permeability band gap, is complex for larger loop radii.

It is well-known that the plasmonic resonance of a metallic nanoparticle is highly sensitive to the dielectric permittivity of the surrounding media (ϵ_b). The plasmonic resonance of a cylindrical nanoparticle occurs

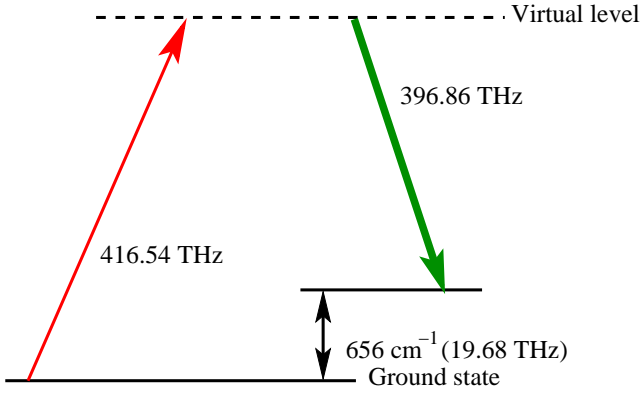


FIG. 8: The proposed level scheme for Inverse Raman Effect in CS_2 .

when the condition

$$\text{Re}[\epsilon_b + \epsilon_m] = 0, \quad (14)$$

is satisfied [30]. Using a Drude form for the permittivity of the metal (ϵ_m), the plasmon resonance frequency of a metallic cylinder may be written as:

$$\omega_r = \omega_p \left[\frac{1}{\epsilon_b + \epsilon_\infty} - \frac{\gamma^2}{\omega_p^2} \right]^{1/2} \quad (15)$$

where ω_r is the plasmon resonance frequency for the nanoparticle, ω_p and γ defines the bulk plasma frequency and the bulk dissipation of the metal, while ϵ_∞ is its ‘static’ permittivity. Hence, even a small change in ϵ_b can shift the plasmon resonance frequency of the nanorod and by extension, the magnetic loop resonance frequency arising out of the circulating displacement current around the loop. We note a subtle difference between the SRR and the plasmonic metamaterial which may affect the efficiency with which their magnetic response is manipulated. In the case of the SRR, the displacement current is confined to the region within the capacitive gaps of the SRR. In this case, however, the displacement current is between adjacent nanoparticles, and hence, spatially delocalized. A more closely packed loop would, in principle, enable a higher degree of localization of currents and a stronger resonant response.

Control of ϵ_b by an applied electromagnetic radiation is the key to the control of the composite metamaterial itself. In order to demonstrate parametric control over the magnetic resonance, an atomic/molecular system exhibiting a resonance in the neighbourhood of the band gap frequency is essential. Raman transitions that provide such resonances can be effectively used in a very flexible manner because the Raman resonance frequency can be tuned by the choice of the pump laser frequency. A strong pump field with frequency ν_0 will create conditions for the resonant absorption of a probe field at a frequency ($\nu_0 + \nu_R$) (Inverse Raman Effect [31, 32]), where ν_R is the molecular level spacing of the medium. We present the calculated results for such a stimulated

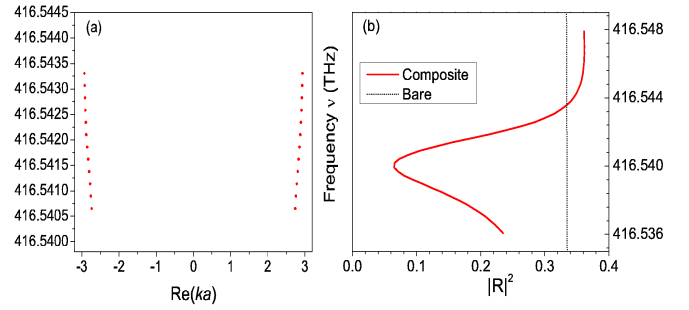


FIG. 9: (a) & (b) The new band formed and the modified reflectivity of the plasmonic metamaterial in the neighbourhood of a Raman transition in CS_2 at 416.54 THz. The vertical line in (b) represents the reflectivity of the bare ‘metamaterial’.

Raman absorption process (Fig. 8) at 416.54 THz in CS_2 with ground state vibrational level spacing of 656 cm^{-1} (19.68 THz). Experimentally obtained values for the parameters of CS_2 were used [33], corresponding to the non-resonant $\chi^{(3)}$ response. We use peak pump powers of the order of 100 GW/cm^2 and a typical linewidth of 0.5 cm^{-1} (15 GHz). Our estimates for the nonlinearity are overtly conservative as the resonant Raman process would be expected to enhance the $\chi^{(3)}$ response. Such inverse Raman absorption of about -15dB has been reported in amorphous silicon by with much lower pump powers of about 1 GW/cm^2 [35], assuming a pump laser field at 396.86 THz which lies within the propagating band of the metamaterial (Fig. 7(a)).

An additional propagating band develops within the band gap region seen in Fig. 7, in the presence of the pump field and this propagating band region has been expanded in Fig. 9 This is manifested by a sharp drop of ($\sim 20\%$) in the reflectivity of the medium. The new band formed is quite dissipative and this prevents a large change in the transmittivity in comparison with the change in reflectivity. The transmittivity of the composite metamaterial is reasonable when compared to that for the ‘bare’ metamaterial, but is completely overshadowed by the large change in the reflectivity. It is possible to numerically demonstrate dramatic enhancement of the transmittivity by several orders of magnitude by using higher pump intensities. Thus, the effect of the introduction of the resonant Raman medium results in a sharp reduction in the reflectivity of the composite metamaterial over a narrow frequency band ($\sim 5 \text{ GHz}$). It is the linewidth of the Raman pump laser that dictates the linewidth of the induced absorption, which in turn determines the change in the reflectivity. The number of propagating bands that are formed are strongly dependent on the resonant nature of the background medium. In the case of EIT-based control, additional bands which switch rapidly between states of low and high transmittivity, are formed in the presence of a control field Ω_c [29].

The behaviour of the metamaterial for radiation of the other state of polarization (with the electric field

of the incident radiation directed along the axis of the metallic rods) may also be controlled in a similar manner [34]. Fig. 6 (a) continues to represent a typical section of the metamaterial, considered here, however, with the \vec{E} field along the nanorod axes. As shown in Ref. [34], the transmittivity of the effective plasma is zero while the reflectivity is high below the cut-off frequency. At higher frequencies, the transmittivity of the medium increases considerably. These correspond to the regions where $\epsilon_{\text{eff}} < 0$ and $\epsilon_{\text{eff}} > 0$, respectively. The response of this metamaterial can be actively manipulated using embedded atomic/molecular media. The introduction of an embedding medium with a resonant response below the effective plasma frequency, into the metamaterial, will drive the effective permittivity to positive values over narrow frequency bands. This results in the formation of transmissive bands below ω_p . Resonant enhancement of the background permittivity can also be achieved by stimulated Raman absorption due to an applied pump radiation in a similar manner. A new transmission band is found to develop at this frequency, which lies below the effective plasma frequency for the medium [34]. We further note that a lower linewidth of the pump laser results in a significant increase in transmittivity. The plasma-like behaviour of the nanorod array depends on a bulk averaging process to determine its overall response and does not necessitate a ‘loop’-like arrangement. Thus, the response of the nanorod array to light of the two orthog-

onal states of linear polarization and their subsequent modified behaviour in the presence of a dispersive permittivity has a different origin.

V. CONCLUSION

We have thus demonstrated a new scheme for the control of metamaterials where the resonant metamaterial response is itself completely transformed by the introduction of controllable resonant media into the design. Coupled with the fact that metamaterials can be designed to show a resonant response at a predetermined frequency, this technique provides an entirely new way of reducing the dissipation in metamaterials, as our results show. We have discussed the control of SRR-based metamaterials by the parametric control of the capacitance, the control of nanorod plasmonic loop metamaterials by the control of the surface plasmon resonance via the background dielectric environment and the control of the plasma-like behaviour of the nanorod metamaterial by changing the bulk average dielectric permittivity. The variety of such possibilities of control demonstrate the generality of this approach. The control scheme presented here enhances the tunability of metamaterials and can be effectively used for a variety of narrow-band applications, thus moving towards dynamically controllable metamaterials.

-
- [1] S. E. Harris, Phys. Today, **50**(7), 36 (1997)
 - [2] L. J. Wang, A. Kuzmich, & A. Dogariu, Nature, **406**, 277 (2000)
 - [3] L. V. Hau, S. E. Harris, Z. Dutton, & C. H. Behroozi, Nature, **397**, 594 (1999)
 - [4] D. F. Philips, A. Fleischhauer, A. Mair, R. L. Walsworth, & M. D. Lukin, Phys. Rev. Lett., **86**, 783 (2001)
 - [5] C. Liu, Z. Dutton, C. H. Behroozi & L. V. Hau, Nature, **409**, 490 (2001)
 - [6] S. E. Harris, J. E. Field, & A. Imamoglu, Phys. Rev. Lett, **64**, 1107 (1990)
 - [7] K. J. Boller, A. Imamoglu, A. & S. E. Harris, Phys. Rev. Lett., **66**, 2593 (1991)
 - [8] M. O. Scully, Phys. Rev. Lett., **67**, 1855 (1991)
 - [9] S. A. Ramakrishna, Rep. Prog. Phys., **68**, 449 (2005)
 - [10] D. R. Smith, W. J. Padilla, D. C. Vier, S. C. Nemat-Nasser, & S. Schultz, Phys. Rev. Lett., **84**(18), 4184 (2000)
 - [11] R. A. Shelby, D. R. Smith, & S. Schultz, Science, **292**, 77 (2001)
 - [12] J. B. Pendry, Phys. Rev. Lett, **85**, 3966 (2000)
 - [13] J. B. Pendry, D. Schurig, & D. R. Smith, Science, **312**, 1780 (2006)
 - [14] V.M. Shalaev, Nature Photonics, **1**, 41 (2007)
 - [15] W. J. Padilla, A. J. Taylor, C. Highstrete, Mark Lee, and R. D. Averitt, Phys. Rev. Lett., **96**, 107401 (2006)
 - [16] J. Han, A. Lakhtakia and C.-W. Qiu, Optics Express, **16**, 14390 (2008)
 - [17] D.H. Werner, D.-H. Kwon, I.-C. Khoo A.V. Kildishev and V.M. Shalaev, Opt. Express **15**, 3342 (2007)
 - [18] S. O’Brien, D. McPeake, S. A. Ramakrishna, and J. B. Pendry, Phys. Rev. B, **69**, 241101 (2004)
 - [19] J. B. Pendry, A. J. Holden, D. J. Robbins, & W. J. Stewart, IEEE Trans. Microwave Theory Tech., **47**, 2075 (1999)
 - [20] A. Alu, N. Salandrino and N. Engheta, Optics Express, **14**, 1557 (2006)
 - [21] S. O’Brien and J. B. Pendry, J. Phys.: Condens. Matter, **14**, 6383 (2002)
 - [22] N. G. Kalugin, & Y. V. Rostovtsev, Optics Letters, **31**, 969 (2006)
 - [23] M.O. Scully and M.S. Zubairy *Quantum Optics*, Cambridge Univ. Press, Cambridge, U.K. (1997)
 - [24] M. I. Stockman, Phys. Rev. Lett., **98**, 177404 (2007)
 - [25] J.B. Pendry and A. Mackinnon, Phys. Rev. Lett. **69**, 2772 (1992)
 - [26] J.B. Pendry, J. Mod. Opt. **41**, 209 (1994)
 - [27] P.B. Johnson and R.W. Christy, Phys. Rev. B, **6**, 4370 (1972)
 - [28] Th. Koschny, P. Markos, D. R. Smith and C. M. Soukolis, Phys. Rev. B, **65**, 195104 (2002)
 - [29] S. Chakrabarti, S. A. Ramakrishna and H. Wanare, Opt. Exp., **16**, 19504 (2008)
 - [30] Lukas Novotny and Bert Hecht, *Principles of Nano-Optics*, Cambridge Univ. Press, Cambridge, U.K. (2006)
 - [31] W. J. Jones and B. P. Stoicheff, Phys. Rev. Lett., **13**, 657 (1964)
 - [32] A. D. Buckingham, The Journal of Chemical Physics, **43**,

- 25 (1965)
- [33] Amnon Yariv, *Quantum Electronics*, John Wiley and Sons Inc. (1989)
- [34] S. Chakrabarti, S. A. Ramakrishna and H. Wanare, *Optics Letters*, **34**, 3728 (2009)
- [35] D. R. Solli, P. Koonath, and B. Jalali, *Phys. Rev. A*, **79**, 053853 (2009)